On Cyber-Physical Coupling and Distributed Control in Smart Grids

Eman Hammad, *Member, IEEE*, Abdallah Farraj, *Senior Member, IEEE*, and Deepa Kundur, *Fellow, IEEE*

***Abstract*—This article focuses on characterizing the impact of communication on distributed control performance in smart grid systems. Using a cyber-physical model of the smart grid and utilizing electromechanical wave propagation in transmission systems, a holistic approach is proposed to unify cyber-physical coupling representation. This is facilitated by establishing an event-propagation paradigm relating measurements, distributed control and the physical power systems network characteristics. We investigate how power system characteristics impose limitations on distributed control performance using the proposed approach. The proposed approach is then used to derive fundamental communication delay limits for effective distributed control, and comparative analysis of distributed control performance is investigated for example distributed control scenarios.**

***Index Terms*—Communication network, coupling, cyber-physical systems (CPSs), distributed control, distributed energy resources, electromechanical (EM) waves, event propagation, graphs, latency, smart grid.**

I. Introduction

TO ENHANCE the reliability of smart grid systems, we continue to witness the advancement of distributed control paradigms that complement existing strategies for wide area monitoring, protection, and control [1], [2]. These developments are highly invested on the availability and performance of communication infrastructures [3]–[5]. Cyber-physical system (CPS) models are used to assess the effectiveness of cyber-enabled control by accounting for interactions between the (physical) power system and (cyber) communication network. Such CPS models exhibit tradeoffs in tractability and modeling granularity due to the distinct nature of cyber and physical domains. To address these challenges, techniques often aim to look at the CPS in an *equivalent* cyber domain or via multi-agent models [6]–[9].

Manuscript received April 23, 2018; revised September 30, 2018; accepted November 30, 2018. Date of publication December 27, 2018; date of current version August 1, 2019. This work was supported by the Natural Sciences and Engineering Research Council of Canada under grant RGPIN 227722. Paper no. TII-18-0989. *(Corresponding author: Eman Hammad.)*

The authors are with the Department of Electrical and Computer Engineering, University of Toronto, Toronto ON M5S, Canada (e-mail: ehammad@ece.utoronto.ca; abdallah.farraj@utoronto.ca; dkundur@ece.utoronto.ca).

Color versions of one or more of the figures in this paper are available online at http://ieeexplore.ieee.org.

Digital Object Identifier 10.1109/TII.2018.2890002

CPS multi-agent models employ, in part, tools from graph theory for the design and convergence analysis of distributed control. For example, a multi-agent dynamical system with existing interaction/coupling between the agents can be modeled using a graph with agents as vertices and weighted links representing inter-agent couplings [8], [9]. Within this context, control convergence speed is shown to be directly related to the *algebraic connectivity* (second smallest eigenvalue of the Laplacian) of the graph model.[1] However, communication links exhibit delays and intermittent availability. This motivated studies investigating the dependence of consensus on communication links performance. The work in [10] shows that consensus can be achieved provided the delay is bounded. Further, delay robustness of consensus is proved in [7] for single integrator multi-agent system with constant, time-varying or distributed delay provided the underlying graph is strongly connected. Above treatments abstract the cyber component as a variable or bounded delay and study the impact from the perspective of the networked control system. These approaches seek to analytically verify robustness of networked control in the presence of unknown and uncertain cyber infrastructure performance. However, they are observed to have rather complex formulations or unexplained empirical limitations [11]–[13].

In another research direction, a general hybrid systems approach is developed to model the dynamics of CPS. Hybrid automata provides a single mathematical formalism that captures both the transition between discrete states in the cyber system, and the evolution of continuous states over time in the physical system [14], [15]. Recent works have applied the hybrid automata approach to study discrete control states/actions in transmission systems and microgrids. While this approach helps verify control design against a set of discrete states, it is rather complex when considered in the distributed formulation. Another treatment that is based on CPS hybrid systems is used to develop a unifying methodology to integrate continuous dynamics with discrete-event approaches [16], [17]. A toolkit (Ptolemy II) is developed to enable a more scalable treatment, which is applied to study cyber computational requirements for distributed energy systems in [18].

Studying cyber-physical interactions in the context of power systems unveils two types of inter-agent couplings: a

[1] A higher algebraic connectivity is correlated to a better connected graph and hence greater coupling between the agents resulting in faster convergence [9].

physical-coupling inherent from the physical connectivity of power system components via transmission lines (TLs), and a cyber-coupling that is introduced through communicated measurements and informed actuation. Interactions between the cyber and physical domains of the smart grid promise improved system operation via cyber-enabled control. However, previous studies observed that these benefits have limitations that can be related to the performance or architecture of the cyber domain [19].

This work focuses on combining cyber and physical interactions between distributed control agents in power transmission systems using a unifying cyber-physical coupling representation. The proposed unifying representation focuses on a common propagation model-based analogy in both cyber and physical domains. To facilitate this, we based on the work in [20]–[22], where power system events are shown to be modeled through an *electromechanical* (EM) wave propagation model. The proposed cyber-physical coupling representation "combines" communication links and physical power system TLs in one graph. Within this representation, a communication link is mapped into an *equivalent impedance*. This work is not a mathematical analysis tool, but rather an intuitive tractable approach to gain insights on limitations imposed on the CPS by the existing power system physical infrastructure.

Contributions of this work can be summarized as: 1) develop an event-propagation paradigm to relate power systems physical-coupling and dynamics with communication links performance; 2) derive cyber-physical coupling representation of communication links, and their dynamic changing performance, based on a physical favoring interpretation; and 3) quantify limitations and impacts imposed by existing physical-coupling on the performance of cyber-enabled distributed control. The cyber-physical coupling graph is used to design an adaptive distributed control for the New England 39-bus systems; and to compare the performance of different distributed control scenarios.

II. Model and Problem Formulation

A. System Model

Within the multi-agent CPS model of the smart grid, physical-couplings stem from the presence of TL connecting agents while cyber-couplings are the result of networked control that harnesses sensors, communications, and information-based decision-making. A control-based perspective is considered in this setup as control exists at the cyber-physical boundary and is effected by each domain. The objective is to relate physical system interactions resulting from cyber-enabled control decisions to develop a unifying representation of cyber and physical couplings. The approach combines the two couplings in a single cyber-physical graph with a defined edge weight that favors a physical system interpretation (impedance). Measurement delays are dynamically mapped as an equivalent impedance enabling a quantitative comparison between cyber and physical couplings.

B. Event-Propagation Paradigm

An event-*propagation* paradigm is proposed based on the realization that both data transmission over communication links and power flow over TLs follow a natural signal propagation model. Interestingly, it has been observed that the dynamics of synchronous generators connected with TLs, in response to disturbances, produce traveling wave-like phenomena termed *EM* waves [20]–[22]. Here, an EM wave originates from each agent traveling across the TL at a speed that is much lower than the speed of light [21], [23], [24].

C. EM Waves

EM wave model considers the classical swing equations that capture synchronous generators dynamics. The swing model is a second-order ordinary differential equation as in (1)[20], [23]

$$\frac{2H}{\omega_s}\frac{d^2\delta}{dt^2}+\omega D\frac{d\delta}{dt}=P_A=P_M-P_E \tag{1}$$

where δ is the generator rotor angle, ω denotes the generator rotor angular speed, D is the generator damping coefficient, and H is the machine's inertia constant. Let Ω_s denote the system nominal angular frequency (typically equal to $60\cdot 2\pi$ or $50\cdot 2\pi$ depending the geographical location). The mechanical and electrical powers of the generator are denoted P_M and P_E, respectively, while the accelerating power is denoted as $P_A=P_M-P_E$.

The EM model developed in [20] and [25] takes a limit of the swing equation model, presenting the power system as a two-dimensional (2-D) uniformly distributed small generators and TLs. Within this context; inertia constant, mechanical damping and line impedance become distributed parameters over the 2-D coordinates (x,y) as

$$\begin{aligned} &H\rightarrow \Delta h(x,y)\quad D\rightarrow \Delta d(x,y)\\ &Z\rightarrow \Delta z(x,y)\quad P_M\rightarrow \Delta p_M(x,y). \end{aligned} \tag{2}$$

Reconsidering (1) with the electric power term expanded as is found in [20], and considering (2) as the limit $\Delta\rightarrow 0$, then the model can be written as a nonlinear hyperbolic wave equation in δ as

$$\frac{\partial^2\delta}{\partial t^2}+\nu\frac{\partial\delta}{dt}-v^2\nabla^2\delta+u^2(\nabla\delta)^2=P \tag{3}$$

where

$$\begin{aligned} \nu&=\frac{\omega^2 d}{2h}\\ v^2&=\frac{\omega V^2\sin\theta}{2h|z|}\\ u^2&=\frac{\omega V^2\cos\theta}{2h|z|}\\ P&=\frac{\omega(p_M-GV^2)}{2h} \end{aligned} \tag{4}$$

where θ is the phase associated with the TL impedance and is close to $\theta=\pi/2$ for high voltage TLs, V is the source voltage

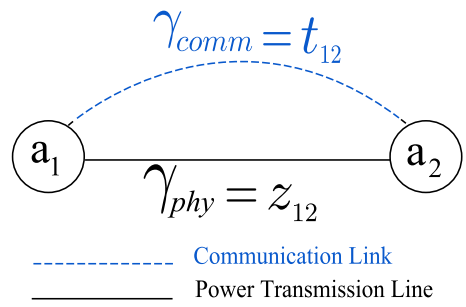

Fig. 1. Two-agent system.

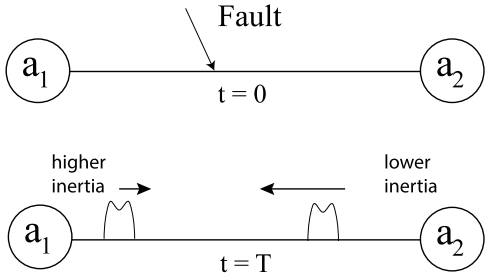

Fig. 2. TL fault initiates EM waves from each agent.

in per unit (taken to be of constant magnitude and variable phase), h is the generator inertia constant per mile and z is the line impedance in per unit per mile, and ∇^2 is the Laplacian operator.[2]

D. Cyber-Physical Coupling: Two-Agent Model

Consider a two-agent system setup as shown in Fig. 1, where an agent represents a synchronous generator with integrated distributed control and associated sensors. Let γ be a coupling metric, and let the physical-coupling between Agents (a_1, a_2) be characterized by the impedance (electrical distance) of the TL connecting the two agents; i.e., $\gamma_{\rm phy} = z_{12}$. A communication link is also present connecting Agents (a_1, a_2) to communicate measurements and enable distributed control; let this cyber-coupling be characterized by the delay of the communication link $\gamma_{\rm comm} = t_{12}$.

When a fault occurs somewhere along the TL, it generates a traveling wave that is sensed almost simultaneously at both agents.[3] Recall that interactions of synchronous machine dynamics in response to the fault are modeled as EM waves initiated (by the traveling waves) at both agents. Here, Agent a_1's EM wave will take time to physically propagate to Agent a_2 (and vice versa), as illustrated in Fig. 2. Impact of the fault will result in each synchronous machine reacting to the fault according to its inertia, if reactions are not addressed by control, then the system could go unstable, two strategies for control prevail: local control and distributed depending on availability of remote measurements. In the absence of communication between the two agents, Agent a_2 can compute its control decision c_2 based on its local measurement m_2; i.e., $c_2 = f(m_2)$ to address the disruption. However, if a sensor measurement m_1 at Agent a_1 can be communicated to Agent a_2 in a timely manner (i.e., at a delay t_{12} that is less than that of the EM wave originating from a_1,), new opportunities can be realized to mitigate disruption through informed control: $c_2 = f(m_1(t_{12}), m_2)$. Hence, the effectiveness of control for mitigation can be significantly enhanced with the presence of a *fast* communication link between physically coupled agents.[4]

The described event-propagation paradigm establishes a context within which communication link performance (cyber-coupling; delay) is related to EM wave propagation speed (physical-coupling, TL impedance, and the inertia of synchronous machines). With this understanding, one can proceed to consider a compatible graph-based metric to describe inter-agent cyber and physical couplings that allows their consolidation into an overall measure of cyber-physical coupling. The objective is to derive a metric that would help determine how cyber connectivity and performance can improve the operation of a physically coupled power system via distributed control.

This discussion highlights two possible domains where cyber and physical couplings may be combined and compared using a compatible metric. A time-delay domain, and a cyber-physical impedance domain. Advantages of adopting a cyber-physical impedance domain include that the impedance representation: 1) is more lucid from a power system perspective; and 2) preserves the physical base of the system that facilitates an energy flow perspective.

Here, the two-agent model is used to illustrate and facilitate the discussion of the main concepts comprising the proposed approach: the event propagation-paradigm, the cyber-physical coupling representation, and later the directional equivalent impedance. This two-agent model enables a more clear and focused discussion of these concepts, as it isolates the two-agent system from other inter-agent interactions in the complete power system, while preserving the main characteristics of the system that are essential to the study. Next, this model is extended into a multi-agent model in the problem formulation.

E. Problem Formulation

Reconsider the multi-agent system comprised of N *agents* that describes an N-generator and M-bus power system. Each agent is comprised of a synchronous generator, a sensor that measures the corresponding generator's variables, and a controller that utilizes local and/or remote sensor measurements to make decisions. Consider the following definitions.

[2]The system of measurement used through the paper is based on the metric system when calculating speeds, delays, and equivalent impedances. However, power system characteristics (e.g., h, z) with respect to the original EM wave propagation model are described based on imperial units to maintain the reference to the original model. Appropriate conversions are applied implicitly where required.

[3]Traveling waves are electromagnetic waves that are initiated by a fault in TLs and travel at nearly the speed of light [26], [27].

[4]This notion is partly observed in standards such as the digital substation IEC61850 GOOSE messaging protocol, where message delay constraints for performance class P2/3 must be within 4 ms [28].

Definition 1 (Physical Graph): Let the power system be described by the weighted connected undirected graph $G_{\rm phy}(V, E, W, f_{\rm phy})$, where the node set V denotes system buses, the edge set $E \subset V \times V$ denotes TLs, and $W \subset \mathbb{R}^+$ presents the edge weights set in impedance units (ohms). Further, $f_{\rm phy} : E \to W$, such that for edge $e_{ij} \in E$, the corresponding weight defined as w_{ij} represents the physical-coupling (impedance) between associated nodes/buses.

Definition 2 (Cyber Graph); Let the communication network connecting power system agents be described by the weighted undirected graph $G_{\rm comm}(\check{V}, \check{E}, \check{W}, f_{\rm comm})$, where the node set $\check{V} \subset V$ denotes power system buses with cyber-enabled control, the edge set $\check{E} \subset \check{V} \times \check{V}$ denotes communication links, and $\check{W} \subset \mathbb{R}^+$ presents the edge weights set in delay units (seconds). Here, $f_{\rm comm} : \check{E} \to \check{W}$, such that for edge $\check{e}_{ij} \in \check{E}$ the corresponding weight defined as $\check{w}_{ij}$ represents the cyber-coupling (delay) of corresponding communication link.

The problem of developing a cyber-physical coupling representation can be formulated as follows.

Given the physical graph $G_{\rm phy}(V, E, W, f_{\rm phy})$ (Definition 1) and communication graph $G_{\rm comm}(\check{V}, \check{E}, \check{W}, f_{\rm comm})$ (Definition 2), then the objective is to define the cyber-physical coupling graph $G_{cp}(\bar{V}, \bar{E}, \bar{W}, f_{cp})$ *through the mapping operator* $\mathfrak{P} : \check{W} \to \bar{W}$. In this graph, the node set $\bar{V} = V$ denotes the cyber-physical graph nodes given by the physical graph buses, the edge set $\bar{E} = (E \cup \check{E})$ is comprised of the union of both the physical TLs and communication links, and $f_{cp} : \bar{E} \to \bar{W}$ assigns each link $\bar{e}_{ij} \in \bar{E}$ to its corresponding weight $\bar{w}_{ij}$ in an appropriate weight set.

Note that for the EM wave propagation and the event-propagation paradigm to hold, cyber-physical Agents i and j must necessarily be connected physically, that is $e_{ij} \in E$.[5] Consequently, each edge $\bar{e}_{ij}$ of the proposed G_{cp} would describe one of three cases related to the type of connections between Agents (i, j): 1) TL only, 2) TL and a communication link, and (3) no connection (cyber or physical). Thus, the link-weight $\bar{w}_{ij}$ can be assigned as follows:

$$\bar{w}_{ij} = \begin{cases} w_{ij} & e_{ij} \in E, \check{e}_{ij} \notin \check{E}, \text{(physical link only)} \\ w_{ij} \oplus \mathfrak{P}(\check{w}_{ij}) & e_{ij} \in E, \check{e}_{ij} \in \check{E}, \text{(cyber and physical links)} \\ 0 & \text{else} \end{cases}. \tag{5}$$

In this context, the mapping operator $\mathfrak{P}$ maps a communication link edge weight to an equivalent impedance that will be further developed and discussed in Section III-C. The *association operator* $\oplus$ defines how to combine the physical impedance and the cyber equivalent impedance, and is further elaborated in Section III-D. Note that the assignment of (5) is well-defined and meaningful because both $\mathfrak{P}(\cdot)$ and w_{ij} are measured in the same physical units.

[5]Two agents are physically connected if there is a path for power flow between them.

III. Cyber-Physical Coupling

In this section, the event-propagation paradigm is extended to arrive at the mapping operator $\mathfrak{P}$.

A. Cyber-Coupling Equivalent Impedance

For a communication link, signal propagation speed v is related to communication delay t and link distance d as follows:

$$v = d/t. \tag{6}$$

Recall how EM waves represent the dynamic response of synchronous generators and TLs to traveling waves emanating from a fault in Section II-C [20], [25]. The EM model in (3) describes the propagation speed $v_{\rm EM}$ as a function of the rotational inertia of the generator and TL impedance as

$$v_{\rm EM} = \sqrt{\frac{\omega V^2 \sin\theta}{2h|z|}}. \tag{7}$$

It should be noted that several research efforts have reported very similar relationships between h, z and estimates of $v_{\rm EM}$ [29]. Further, multiple system setups and simulations in [20]–[22] have confirmed an EM wave propagation speed that is very similar to (7), where the speed is inversely proportional to generator inertia and TL impedance.

Hence, agents in the physically coupled power system are able to sense variations in system dynamics in response to physical events through the EM wave propagation model. From the distributed control perspective, receiving remote measurements from the same physically coupled agents that convey the variations in system dynamics at each of the agents can be viewed as another "virtual" EM wave. This "virtual" EM wave arrived the distributed control after experiencing some communication delay related to the performance of the communication link at that time. Hence, the "virtual" EM wave had a propagation speed equal to that of the communication link.

Hence, equating (6) to (7), a measurement delay over a communication link t can be related to a cyber-coupling *equivalent impedance* $\hat{z}$ as

$$\hat{z}(t) = \frac{t^2 \omega V^2 \sin\theta}{2d^2 h}, \hat{z} \in \mathbb{R}_{\geq 0}. \tag{8}$$

The proposed model abstracts all communication technologies into a measurement-based characterization of any communication link based on its inferred delay and distance. It should also be noted that this delay is a varying quantity that changes based on the state of the communication link. This model assumes the existence of a telemetry infrastructure with mechanisms/technologies to enable accurate time-stamping of system measurements. With this infrastructure, the distributed controller will be continually receiving remote agents measurements, and calculating associated communication delays based on the measurements' time-stamps. The reader should note that unlike a physical impedance, $\hat{z}(t)$ is a positive *real* measure reflecting the degree of cyber-coupling.

1) Example: To obtain an insight into how measurement delays over a specific communication link would translate to an equivalent impedance, we consider the example provided

in [20] of the two-agent system of Fig. 1. Here, $\theta = \pi/2$ and $V = 1.0$ pu. The base impedance $Z_{\text{base}} = 500^2/100 = 2500$ Ω for a base power of $S_{\text{base}} = 100$ MVA and base voltage of 500 kV. Taking the inertia constant to be $h = 6$ s per mile, and the line impedance $z = 0.8/2500 = 3.2 \times 10^{-4}$ pu per mile, the EM propagation speed is evaluated to be $= 500 \times 10^3$ m/s.[6] This is much lower than the speed of light (3×10^8 m/s).

Let the TL length be $d = 125$ km, which would result in an EM propagation delay of $t = 125/500 = 250$ ms. Consider a fiber optic communication channel conveying information over the same geographical distance d. For a perfect channel with no other delays, other than propagation delay, then system measurements on this communication link will exhibit a delay of $t = 0.41667$ ms. Applying (8), it is found that the cyber-coupling equivalent impedance $\hat{z}(t = 0.41667) = 3.4907 \times 10^{-6}$ pu per mile. A comparison between the TL impedance and the cyber-coupling equivalent impedance shows the dominance of the cyber for the aforementioned measurement delay values.

B. Directional Equivalent Impedance

Based on (7), we recognize the possible existence of two EM waves on each physical link that are traversing the TL at different speeds in opposing directions. This was observed by another study in [24] where it was noted that EM waves propagate at different speeds in different directions of the TL. Again, (7) captures this observation as EM wave source generators typically have different inertia (while other characteristics are similar), thus the resulting EM wave from either generator will have a different propagation speed.

Hence, the two-agent system will exhibit two (possibly distinct) *directional* equivalent impedances $\hat{z}_{12}$ and $\hat{z}_{21}$ such that $\hat{z}_{ij}$ is the equivalent *directional* impedance from Agent i to Agent j. Let $h_1 > h_2$ denote the inertia constant of the generators at a_1 and a_2, respectively. One can infer from (7) that $v_{\text{EM1}} < v_{\text{EM2}}$.

Next, the following observations are considered to arrive at a non-directional cyber equivalent impedance.

1) Within the perspective of the distributed control, the goal of informed decision making is to act pre-emptively in comparison with the propagation of events in the physical system. This is enabled via received local and remote measurements (recall the two-agent model).
2) However, the communication delay is a non-directional quantity and is unified for that communication link.
3) Hence, this offers a guideline for the correlation between the communication delay and the EM wave delay, where the distributed control would want to be informed of events ahead of any of the two EM waves (i.e., faster than the fastest EM wave).
4) Using (8) for the two EM waves, and then using the observation that the EM emanating from the source generator with the lower inertia would be faster, we embed that understanding to extend (8) to the model in (9).
5) Beyond the maximum delay value that will be calculated based on the derived model in (9), the CPS is shown to be operating as if the measurements are not informative. A more elaborate discussion on this is included in Section III-D2.

In summary, measurements should be communicated faster than the EM wave with the highest speed (related to the lowest inertia). This enables considering a non-directional equivalent impedance $\tilde{z}_{12}$ (in pu per mile) or admittance $\tilde{y}_{12}$

$$\tilde{z}_{12}(t_{12}) = \frac{1}{\tilde{y}_{12}} = \frac{t_{12}^2 \omega V^2 \sin\theta}{2d^2 \min(h_1, h_2)}. \tag{9}$$

Hence, the admittance (in pu)

$$\tilde{Y}_{12}(t_{12}) = \frac{1}{\tilde{z}_{12} d} = \frac{2d \min(h_1, h_2)}{t_{12}^2 \omega V^2 \sin\theta}. \tag{10}$$

C. Mapping Operator $\mathfrak{P}$

The mapping operator $\mathfrak{P}$ referenced in (5) is specifically defined by (10) for corresponding cyber links in the system. Mathematically, for the cyber link between Agents (a_1, a_2) where $\breve{w}_{12} = t_{12}$, and $h_1, h_2 > 0$

$$\mathfrak{P}(\breve{w}_{12} = t_{12}) = \tilde{Y}_{12}(t_{12}) = \frac{1}{\tilde{z}_{12}(t_{12}) d} = \frac{2d \min(h_1, h_2)}{t_{12}^2 \omega V^2 \sin\theta} \tag{11}$$

$$\bar{Y}_{12}(t_{12}) = Y_{12} \oplus \tilde{Y}_{12}(t_{12}). \tag{12}$$

D. Communication Delay

From (9) and (10), it is clear that computing the cyber equivalent impedance (admittance) requires knowledge of the measurement delay over the communication link. Assuming network time synchronization mechanisms are in place, then dynamically obtaining delay information from measurements will be based on calculating the difference between the time the associated measurement was time-tagged and the time its packet was received and ready for computation. Note that EM wave speeds for a certain power system are constant and characteristic of the specific system, while the equivalent admittance is a function of the communication link performance, which is dynamically changing.

1) Timely Measurements: Recall that for a communication link to be effective for distributed control as depicted in Fig. 1, it must transmit measurement data more rapidly than the physical link's faster EM wave propagation speed (given by (7) for $h = \min(h_1, h_2)$). This guarantees that the measurement inputs for control are timely. Similarly, for a general multi-machine power system, it can be deduced that there will be a maximum communication latency/delay bounded by the respective EM wave propagation speeds. Hence, the maximum delay $t_{ij}^{\max}$ for a given communication link between Agents a_i, a_j can be obtained when $v = v_{\text{EM}}$ on that link, and is expressed as

$$t_{ij}^{\max} = \frac{d_{ij}}{v_{\text{EM}}} = \frac{d_{ij}}{\sqrt{\frac{\omega V^2 \sin\theta}{2 \min(h_i, h_j)|z|}}} \tag{13}$$

where d_{ij} and v_{EM} represent the geographic distance and fastest EM wave speed on the corresponding TL, respectively. Thus, communication links experiencing measurement delays greater

[6]These values are based on typical power transmission systems parameters.

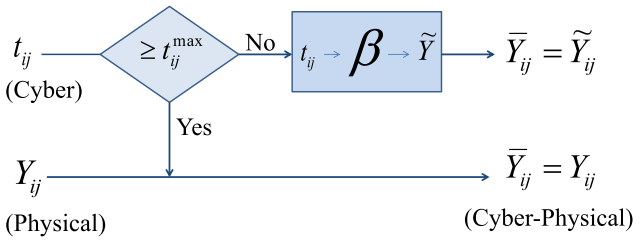

Fig. 3. Flow-chart of the cyber-physical coupling representation model for smart grids.

than $t_{ij}^{\max}$ would not meet the necessary timing guarantees for control. This concept can be utilized to arrive at fundamental limits of communication delays for distributed control in transmission systems.

2) Delay Range and Equivalent Admittance: Given the control logic at Agent a_i, and maximum delay $t_{ij}^{\max}$, lets discuss how communication delay t_{ij} affects $\mathfrak{P}(t_{ij}) = \tilde{Y}_{ij}$ and $\bar{Y}_{ij}$.

1) $t_{ij} \rightarrow 0$: Zero delay could be described as $\tilde{v}_{ij} \gg v_{\text{EM}}$; thus, resulting in $\tilde{z}_{ij} \rightarrow 0$ ($\bar{Y}_{ij} = \tilde{Y}_{ij} \rightarrow \infty$), which clearly dominates the physical-coupling and results in an infinitely coupled two-agent CPS.
2) $t_{ij} \in (0, t_{ij}^{\max})$: Within this range, the overall cyber-physical coupling between the two agents is dominated by the cyber coupling; i.e., $\bar{Y}_{ij} = \tilde{Y}_{ij}$. The cyber equivalent admittance $\tilde{Y}_{ij}$ can be evaluated according to (10), which will be larger than Y_{ij}.
3) $t_{ij} \in [t_{ij}^{\max}, \infty)$: Within this range, delays will result in measurements that are not informative to the distributed control. Hence, the coupling of the CPSs reduces to the original physical-coupling; i.e., $\bar{Y}_{ij} = Y_{ij}$. This delay range is usually the opportunity where switching to local control would be most useful.

One can observe that the cyber-physical coupling simplifies to dependence on either cyber or physical coupling based on which is stronger in the cyber-physical domain. Hence, the association operator $\oplus$ relating cyber-physical "virtual" coupling to cyber and physical couplings over the range of communication delays $t_{ij} \in (0, \infty)$ can be expanded as

$$\bar{Y}_{ij}(t_{ij}) = Y_{ij} \oplus \tilde{Y}_{ij}(t_{ij}) = \begin{cases} \tilde{Y}_{ij}(t_{ij}) & , t_{ij} \in (0, t_{ij}^{\max}) \\ Y_{ij} & , t_{ij} \in [t_{ij}^{\max}, \infty) \end{cases}. \tag{14}$$

Note however that the physical-couplings of a certain power system are characteristic constants of the system (provided there are no topological changes. Meanwhile, the cyber equivalent admittance is a dynamic quantity that can be updated as the controller obtains communicated measurements. Hence, the cyber equivalent admittance reflects different conditions that may impact the communication channel in a simplified approach, such as congestion, outages or denial of service cyber attacks. The proposed approach is illustrated in Fig. 3.

IV. Case Studies

We consider two case studies to illustrate how the proposed approach can be used for useful insights. Case study 1 involves the design of adaptive distributed control based on the identification of maximum communication delay bounds. Cyber-physical coupling in case study 2 facilitates an understanding and prediction of the performance of different distributed control scenarios.

The simulation environment used for the below case studies is developed using Mathworks MATLAB R2016a and Simulink on a Windows 10 64-bit machine with a 2.53-GHz Intel Core i5 CPU and 8-GB RAM.

A. Case Study 1: Adaptive Cyber-Enabled Control

Let us consider the case of cyber-enabled distributed control actuating an energy storage systems (ESS) to address transient stability issues in power transmission systems. The multi-agent cyber-physical model is used to capture the dynamics of the systems, where each cyber-physical agent is composed of: 1) a synchronous generator, 2) a sensor that measures local generators' rotor speed and angle, 3) a distributed controller that receives sensor data from system agents, and 4) a fast-acting ESS[7] that can inject or absorb real power depending on the control signal value. A communication network connects the different cyber-physical agents. The controller affects the dynamics of the power system by actuating the local ESS. The agents are coupled physically by TLs and in cyber form by the communication network. In this model, the physical dynamics of each cyber-physical agent depend on its own state as well as the states of other agents in the system.

1) Cyber-Enabled Control for Transient Stability: Power system stability is defined as the ability of the system to regain a state of equilibrium after being subjected to a physical disturbance [31]. Transient stability describes the ability of the power system to remain in synchronism when subjected to large disturbances [32]. Through application of control techniques, transient stability can be achieved following a physical disturbance by maintaining both speed synchronization and phase angle cohesiveness [31].

For the ith generator, where $i \in \{1, \ldots, N\}$, the generator parameters and states are listed in Table I. We adopt the two-axis sub-transient machine model, which is widely used to capture the dynamics of synchronous generators during transients. The electrical dynamics of Generator i's stator are modeled as [33]–[35]

$$\dot{E}'_{qi} = \frac{1}{T'_{di}} \left(-E'_{qi} - (X_{di} - X'_{di}) I_{di} + E_{fi} \right) \tag{15}$$

$$\dot{E}'_{di} = \frac{1}{T'_{qi}} \left(-E'_{di} + (X_{qi} - X'_{qi}) I_{qi} \right) \tag{16}$$

$$E'_{qi} = V_{qi} + R_{ai} I_{qi} + X'_{di} I_{di} \tag{17}$$

$$E'_{di} = V_{di} + R_{ai} I_{di} - X'_{qi} I_{qi} \tag{18}$$

[7]Example fast-acting ESSs include flywheels [30]).

TABLE I
MACHINE PARAMETER DESCRIPTION

Parameter	Description
E'_d	d-axis transient electromotive force (emf)
E'_q	q-axis transient emf
E_f	field voltage
I_d	d-axis component of stator current
I_q	q-axis component of stator current
R_a	armature resistance
X_d	d-axis synchronous reactance
X_q	q-axis synchronous reactance
X'_d	d-axis transient reactance
X'_q	q-axis transient reactance
T'_d	d-axis transient open loop time constant
T'_q	q-axis transient open loop time constant
T_E	electromechanical torque
T_M	mechanical torque
V_d	d-axis terminal voltage
V_q	q-axis terminal voltage

TABLE II
FAULT DETAILS

Fault Case	Faulted Bus	Tripped Line
1	17	17–18
2	11	10–11
3	22	21–22
4	5	5–8

where $\dot{E}'_{qi}$ and $\dot{E}'_{di}$ denote the time derivative of E'_{qi} and E'_{di}, respectively.

The rotor dynamics of the synchronous generator can be expressed by [33]

$$\dot{\delta}_i = \Omega_s(\omega_i - \omega_s) \tag{19}$$

$$\dot{\omega}_i = \frac{\omega_s}{2H_i}\left(T_{Mi} - T_{Ei} - D_i(\omega_i - \omega_s)\right) \tag{20}$$

where $\dot{\delta}_i$ and $\dot{\omega}_i$ are the time derivatives of δ_i and ω_i, respectively. Further, the field voltage of a generator is controlled by the excitation control system, while the mechanical torque is controlled by the governor. The EM torque is calculated as [33]

$$T_{Ei} = E'_{di}I_{di} + E'_{qi}I_{qi} + (X'_{qi} - X'_{di})I_{di}I_{qi}\,. \tag{21}$$

recall that P_{Mi} and P_{Ei} are the mechanical and electrical powers of Generator i, respectively, and note that $P_{Ei} = T_{Ei}$ and $P_{Mi} = T_{Mi}$ when using per unit representation. Then, the dynamics of the rotor speed in relation to the mechanical and electrical powers (in per unit) are modeled as

$$\dot{\omega}_i = \frac{\omega_s}{2H_i}\left(P_{Mi} - P_{Ei} - D_i(\omega_i - \omega_s)\right). \tag{22}$$

Typically, the accelerating power of Generator i $P_{Ai} = 0$ during normal operation, but when a major disturbance occurs in the power system, the accelerating power of some generators deviates from 0. A large deviation in rotor speed may damage the synchronous machine if not tripped by out-of-step protection [32]. Consequently, a generator might be disconnected from the power grid. A generator is said to be stabilized if its rotor speed is driven back to the synchronous speed and when the rotor phase angle differences of the different synchronous generators are below a predefined threshold. Hence, the primary goal of control addressing transient stability is to intervene quickly to prevent out-of-step tripping of generators until other control mechanisms such as governors are functioning and can drive the system to stability. Traditional control schemes such as excitation and governor control systems typically exhibit slow reaction to rapid changes in the power system dynamics. Fast reacting ESS and the availability of communication provided a good setup to develop advanced control paradigms to help improve the transient stability of the power system.

Cyber-enabled distributed control schemes rely on the existence of a communication network to communicate system state information. Sensor readings are periodically communicated to distributed controllers. The ESS-based distributed control is able to shape the dynamics of the power system by absorbing or injecting defined amounts of real power at specific generator buses.[8] Incorporating the ESS actuation, described via u_i, at the bus of Generator i modifies the swing equations in (19) and (20) at time t to

$$\begin{aligned}\dot{\delta}_i(t) &= \Omega_s(\omega_i(t) - \omega_s)\\ \dot{\omega}_i(t) &= \frac{\omega_s}{2H_i}\left(P_{Ai}(t) - D_i(\omega_i(t) - \omega_s) + u_i(t)\right).\end{aligned} \tag{23}$$

2) Parametric Feedback Linearization (PFL) Control: ESS-based control (u_i) actuates the associated ESS to achieve transient stability; a positive (negative) u_i value in (23) indicates that the ESS injects (absorbs) real power from the bus of Generator i. Let the capacity of the ESS of Agent i at time t be denoted $C_i(t)$. Given $\hat{u}_i$ as the computed control signal (from any of the proposed controllers), then $\hat{u}_i$ is applied to the following model to account for the capacity limits of the local storage system and calculate u_i as

$$u_i(t) = \begin{cases} C_i(t) & \hat{u}_i(t) > C_i(t)\\ \hat{u}_i(t) & -C_i(t) \le \hat{u}_i(t) \le C_i(t)\\ -C_i(t) & \hat{u}_i(t) < -C_i(t).\end{cases} \tag{24}$$

In the presence of measurement uncertainties (due to interference, noise, sensor equipment bias/saturation or false data injection), the PFL controller can be shown to stabilize provided the introduced error is bounded.

3) Centralized Control Architecture: For a centralized PFL control, the controller requires system measurements from all generators in the system to calculate its signal. A centralized PFL control is modeled as [36], [37]

$$\hat{u}_i(t) = -P_{Ai}(t) - \alpha_i(\omega_i(t) - \omega_s) \tag{25}$$

where $\alpha_i \ge 0$ is called the frequency stability parameter. The centralized control aims to cancel the nonlinear terms in the swing equation. Hence, the PFL control signal reshapes the dynamics of the closed-loop power system as a series of stable decoupled linear systems with tunable eigenvalues. Once $\hat{u}_i$ is calculated, the centralized ESS-based controller actuates the associated ESS according to (24).

[8]Transient stability control first addresses rotor speed deviations. Once rotor speed is stabilized, then rotor angle differences between system generators become constant.

TABLE III
NEW ENGLAND POWER SYSTEM MAXIMUM COMMUNICATION DELAY VIA EM WAVE PROPAGATION (S)

No.	1	2	3	4	5	6	7	8	9	10
1		0.2226	0.2512	0.2927	0.4693	0.3383	0.3192	0.2213	0.3270	0.2112
2	0.2226		0.2804	0.4258	0.6828	0.4593	0.4644	0.4494	0.5392	0.3771
3	0.2512	0.2804		0.3892	0.6242	0.4499	0.4245	0.4285	0.5404	0.3926
4	0.2927	0.4258	0.3892		0.2624	0.2883	0.3000	0.4022	0.4096	0.3436
5	0.4693	0.6828	0.6242	0.2624		0.4623	0.5007	0.6764	0.6568	0.5510
6	0.3383	0.4593	0.4499	0.2883	0.4623		0.2063	0.4215	0.4714	0.3972
7	0.3192	0.4644	0.4245	0.3000	0.5007	0.2063		0.4566	0.4467	0.3748
8	0.2213	0.4494	0.4285	0.4022	0.6764	0.4215	0.4566		0.3104	0.2101
9	0.3270	0.5392	0.5404	0.4096	0.6568	0.4714	0.4467	0.3104		0.3312
10	0.2112	0.3771	0.3926	0.3436	0.5510	0.3972	0.3748	0.2101	0.3312	

4) Decentralized Control Architecture: A decentralized ESS-based control is typically used when there is no cyber connectivity between agents, hence a controller relies on local measurements to compute the control signal. $\hat{u}_i$ [38]

$$\hat{u}_i = -(\alpha_i \omega_i). \tag{26}$$

Since decentralized PFL control utilizes local measurements only, the accelerating power term (P_{Ai}) cannot be estimated and consequently cannot be canceled, resulting in a partially linearized control system. This may result in longer time duration to stabilize associated generators.

5) Cyber-Physical Coupling and Timely Measurements: As discussed earlier, as remote measurements are delayed more and more, they become less informative for cyber-enable control. The proposed event-propagation paradigm and the cyber-physical coupling helped identify measurement delay values ($t_{ij}^{\max}$), beyond which the control would require other mechanisms to stabilize the power system. It is important here to note that the above maximum delay $t_{ij}^{\max}$ is a function of physical power system quantities h, z that are characteristic of the power system in study. Hence, the bounds imposed on the performance of communication (acceptable delay) are related to fixed properties of the power system.

In summary, for a certain power system, the maximum measurement delays between each two agents can be evaluated using the proposed approach. A centralized PFL control would rely on remote measurements to address transient stability following disturbances. An outage in the communication link that might be caused by a cyber attack or change in operational conditions will result in delayed or absent measurements. To address this, the design of the distributed control can be adjusted to reflect this understanding. Using the calculated $t_{ij}^{\max}$ values, an adaptive PFL control can be defined.

6) Adaptive Centralized-Decentralized Control: While a centralized control is efficient, it remains highly vulnerable to substantial delays or absence of sensor measurements. Hence, a simple adaptive control combining centralized and decentralized PFL controller designs is proposed as a mediator solution when communication latency or cyber attacks impact the availability of measurements. Let $t \geq 0$ be the latency between the sensors and the controller, and let $t^{\max *}$ denote the worst case maximum latency for the whole power system (lowest value), below which the centralized PFL control can effectively stabilize the system. The proposed centralized-decentralized PFL control can then be described as [39]

$$\hat{u}_i = \begin{cases} -(P_{a,i} + \alpha_i \omega_i) & \text{if } t < t^{\max *} \text{ (centralized)} \\ -(\alpha_i \omega_i) & \text{if } t \geq t^{\max *} \text{ (decentralized).} \end{cases} \tag{27}$$

It is important to observe that the centralized-decentralized PFL control waits until $t^{\max *}$ before activating the decentralized PFL control, and this results in a considerable deviation in the system state following the disturbance. To address this issue, the PFL stability parameter α_i can be adjusted (increased) for a more aggressive control action to stabilize the power system. Or the adaptive control design can choose to implement a delay safety margin T_s, where the centralized control activates the decentralized control at a measurement delay $= t^{\max *} - T_s$ to avoid extreme deviations in system state.

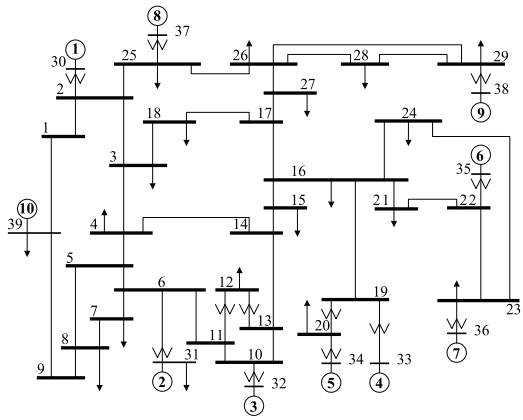

Fig. 4. New England 39-bus 10-generator power system.

7) Numerical Results: Consider the New England power system as shown in Fig. 4. Using the proposed event-propagation paradigm and the cyber-physical coupling representation as in Section III-D1 and (13), maximum communication delays for the New England power system can be analytically calculated and enumerated in Table III. For the corresponding calculations let $z = 0.008$ pu per mile, $V = 1.0$ pu, base voltage $= 100$ kV and $\theta = \pi/2$.

For the New England system, the lowest maximum communication delay is found via the proposed approach to be $t^{\max *} = 206$ ms. Considering a centralized PFL controller where measurements from all agents are required for the control decision, the analytically calculated limit suggests that the communication delay must be less than 206 ms for the PFL control to be able to stabilize the system.

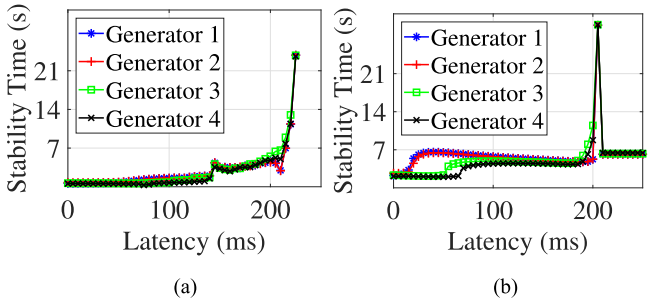

Fig. 5. Performance of the centralized, and adaptive PFL control versus measurement latency. (a) Centralized, fault Case 4. (b) Adaptive centralized-decentralized, fault Case 1.

To verify this, we simulate the performance of the centralized PFL versus measurements latency for the New England power system. As is illustrated in Fig. 5(a), the control is not able to stabilize the power system beyond $t^{\max *} = 206$. Hence, the characteristics of the New England power system with the proposed approach enabled the identification of a maximum communication link delay for the specific power system. Provided the maximum communication link is known, an adaptive centralized-decentralized PFL control can be utilized to ensure that the system is stabilized even if communication delays extend beyond this value. The adaptive centralized-decentralized PFL control is described in (27), and switches to decentralized local control when measurements delays $\geq t^{\max *}$. The improved transient stability of the system versus measurements delays is illustrated in Fig. 5(b).

It is useful here to note that given the current communication technologies, delays remain a challenge for power system's wide area measurements and control. The proposed approach identifies that the characteristics of a certain power system impose hard limits on the performance of communication links.

B. Case Study 2: Performance of Distributed Control Scenarios

Next, consider how the proposed cyber-physical coupling representation graph can help understand and analyze communication impact on distributed control performance. Reconsider Cyber-enabled PFL control, with distributed operations scenarios [40] and investigate how the proposed work can provide an insight in comparing the performance of the various scenarios.

1) Distributed PFL (DiPFL) Control: The DiPFL relies on receiving timely measurements from neighboring generators within a defined control area to compute control decision. Let the N-machine power system be partitioned into areas S_j where $S_j \subseteq N, j = 1, 2, 3, \ldots$, and $S_j \cap S_k = \emptyset$. Mathematically, DiPFL control for rotor speed stability is formulated as a two-level control for each area [41]. Frequency is controlled with a feedback linearization, in the first level, against a dynamic reference frequency $\hat{\omega}$

$$\hat{u}_i = -\alpha_i(\omega_i - \hat{\omega}). \tag{28}$$

A proportional controller is used at the second level to eliminate static errors due to noise and equipment bias as

$$\dot{\hat{\omega}}_i = \gamma_i \left(\omega^{ref} - \frac{1}{|S_j|} \sum_{i \in S_j} \omega_i \right) \tag{29}$$

where $\alpha_i \geq 0$ is the speed stability parameter. $\gamma_i > 0$ is the control update ratio and $\omega^{ref} = 0$ is the normalized reference speed. Equations (28) and (29) define how the underlying consensus algorithm in DiPFL reaches agreement through agent updates in defined areas, such that the system is driven to transient stability with the desired normalized reference frequency ω^{ref}.

DiPFL control can be implemented in various scenarios with different communication topologies and distinct availability of resources (e.g., ESS) at the generators. In the following, when a measurement exchange is required between two agents, we relate that to a direct communication link between the two agents.[9] Three possible scenarios are described below.

1) **Scenario** A**:** Where all generators in area S_j apply the DiPFL control as defined in (28) and (29). Scenario A requires measurements to be communicated between all generators of a control area.
2) **Scenario** B**:** The generator with the largest inertia in each area, designated the head generator, which employs the measurements from all other generators in its area to calculate the control output. This scenario requires measurements to be communicated between the head generator of an area and the remaining generators in its control area.
3) **Scenario** C**:** A *hierarchical control* scenario where the head generator in an area applies a centralized PFL control, while the remaining generators apply DiPFL. Scenario C requires hierarchical communication connectivity with the communication network as described in Scenario A, with additional communication links between all the head generators.

Control areas S_j are identified using a model-based spectral clustering approach, utilizing the admittance matrix of the power system. Recall that the admittance matric for a lossless power systems conforms to the structure of a weighted undirected graph Laplacian matrix [42], [43]. This technique identifies which generators have better a physical-coupling between themselves than with other generators. This enables distributed control to consider various information flow designs to improve the overall performance of the control.

2) Cyber-Physical Coupling and Performance of Distributed PFL Scenarios: Traditionally, the connectivity of the underlying graph presents a measure of the convergence performance of consensus-based distributed algorithms. This is directly related to the second smallest eigenvalue λ_2 (algebraic connectivity) of the graph Laplacian. A higher value of λ_2 implies a more connected/coupled graph, hence distributed consensus algorithms will be able to achieve a faster convergence. Spectral clustering results enable the power system to be viewed as areas (clusters) with stronger physical-coupling between the nodes inside

[9]For power transmission systems, it is often the case that a fiber optics communication link is installed along the TL, hence facilitating an infrastructure that enables direct communication between agents.

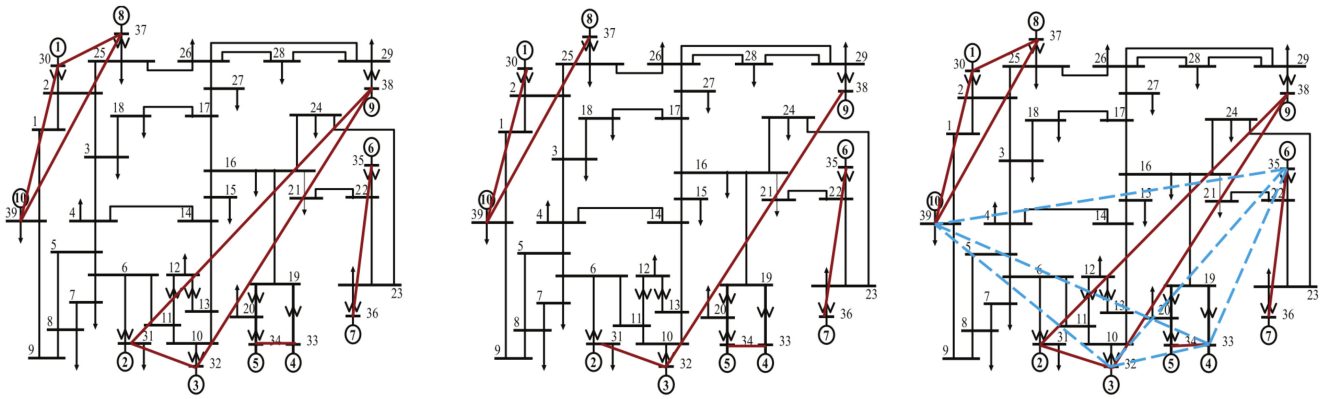

(a) (b) (c)

Fig. 6. Cyber-physical coupling representation graph for New England power system. (a)–(c) Single line diagrams with added communication links for Scenarios A, B, and C, respectively.

TABLE IV
DiPFL-Average Stability Time (s)

	DiPFL Control		
Fault	Scenario A	Scenario B	Scenario C
1	4.4152	17.8172	8.9204
2	4.4215	19.3828	7.0097
3	4.2876	18.6713	6.5167
4	4.2575	19.1858	7.3502

an area and weaker coupling between the different areas. For the considered distributed PFL control scenarios, corresponding communication links have been added to the power system. The added communication links are mapped as equivalent impedances/admittances in the cyber-physical coupling graph. Hence, the distributed control scenarios can now be interpreted as having the following approaches.

1) Introduce communication links to further enhance internal coupling (intra-cluster) of subgraphs/clusters; hence, enabling a faster convergence of each subsystem.
2) Introduce communication links to enhance the connectivity between subgraphs/clusters (inter-cluster) to enable faster convergence of the overall system.

A single line diagram of the three distributed PFL scenarios with corresponding communication networks is presented in Fig. 6. Solid communication lines present intra-cluster links, while blue dashed lines present inter-cluster links.

3) Numerical Results: Spectral clustering of the New England power system, with number of clusters $= 4$ results in 4 control areas. DiPFL performance is evaluated for the three scenarios (A, B, and C). Four cases of disturbances are considered where the power system is assumed to be running in normal state from $t = 0$ to $t = 0.5$ s. A three-phase fault occurs at the faulted bus at $t = 0.5$ s, then the fault is cleared at $t = 0.6$ s. Finally, the control is activated on corresponding generators at $t = 0.7$ s. Table IV enumerates stability results observed for the three distributed PFL control scenarios in the presence of different fault cases. The four fault cases are described in Table II. It is observed that Scenario A performs best in terms of average time to stabilize the system, followed by Scenario C while Scenario B performs poorly in comparison.

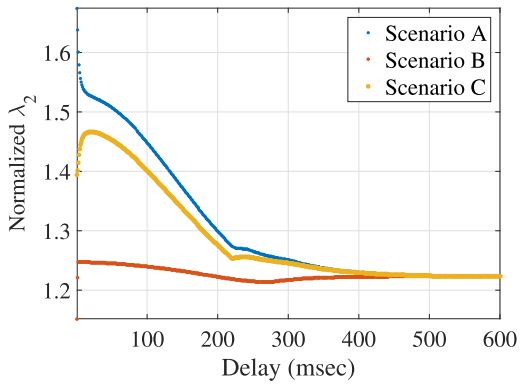

Fig. 7. Algebraic connectivity of the normalized cyber-physical graph Laplacian for the three distributed control scenarios versus measurements delay.

Next, the proposed approach is utilized to evaluate the cyber-physical coupling for the three DiPFL scenarios. This would require obtaining measurement delays, which can be calculated from communicated measurements. However, for the purpose of this study, and due to lack for real system measurements, the following is estimated to induce variable practical delay values in measurements. A specific communication technology that has a defined propagation speed bound (i.e., fiber optics) is assumed, and the corresponding channel propagation delay t_{prop} is calculated using (6). Delays corresponding to average sensory and transmission technology are further added.

Recall that a base MVA of 100 MVA and base voltage of 100 kV would result in a base impedance of $100^2/100 = 100\ \Omega$. Consequently, the per unit per mile impedance is $|z| = 0.8/100 = 0.008$. Using above delay values, along with the New England power system parameters, the corresponding communication equivalent impedances can be evaluated for the system at certain time t. The connectivity of the cyber-physical coupling representation graph is evaluated using the graph algebraic connectivity λ_2 corresponding to each scenario.

This analysis is extended to study how variable communication delay affects the connectivity of the cyber-physical coupling graph. Fig. 7 illustrates the results for the three distributed

control scenarios. It can be observed that the graph is able to provide a relative prediction of the performance of the different distributed PFL scenarios similar to the results obtained by the power system simulation in Table IV. Scenario A and Scenario C are outperforming Scenario B within the noted time delay. It can also be observed that after a certain delay all three scenarios converge to similar connectivity, where the cyber-physical coupling graph reduces to the physical coupling between the different agents. Last, it is noted that Scenario B connectivity is less sensitive to changes in communication delay and that can be useful in related system setups.

V. Conclusion

A cyber-physical coupling representation is presented in this paper to describe the combined effects of cyber and physical coupling between power system agents that is amenable to distributed control. The graph is based on an event-propagation paradigm that provides insight on mapping communication link performance measures such as delay to a metric analogous to an equivalent physical electrical distance (impedance). Numerical results using the New England 39 bus system illustrated how the proposed approach allows computing characteristic upper bounds on communication delay for effective networked control of the system. The delay bound were used to design adaptive distributed control. Further, it enabled the understanding and prediction of the performance of different distributed control scenarios.

Advantages of the proposed event-propagation paradigm and cyber-physical coupling representation graph are as follows.

1) It treats communication links in terms of delay that is observable from time-stamped measurements and hence easily and practically measurable, which allows for dynamically evaluating various communication technologies and topologies.
2) It presents communication impact in a form comprehensible from a power systems perspective.
3) It invests in an understanding of the system component dynamics and interactions.
4) It establishes a systematically quantifiable equivalence of communication links that can be investigated using exiting tools such as graph-theory, which were not previously amenable to application within the same context.

In summary, the presented work illustrated how existing physical power system characteristics impose limitations on the extent of improvement offered by communication and cyber-enabled components. This observation can be used in combination with the presented work to investigate co-design approaches for an optimal cyber-physical coupling.

References

[1] M. Andreasson, "Control of multi-agent systems with applications to distributed frequency control of power systems," Licentiate Thesis, School Electr. Eng., KTH, Stockholm, Sweden, Mar. 2013.

[2] A. Farraj, E. Hammad, and D. Kundur, "On the use of energy storage systems and linear feedback optimal control for transient stability," *IEEE Trans. Ind. Informat.*, vol. 13, no. 4, pp. 1575–1585, Aug. 2017.

[3] Q. Yang, J. A. Barria, and T. C. Green, "Communication infrastructures for distributed control of power distribution networks," *IEEE Trans. Ind. Informat.*, vol. 7, no. 2, pp. 316–327, May 2011.

[4] D. Ghosh, T. Ghose, and D. K. Mohanta, "Communication feasibility analysis for fmart grid with phasor measurement units," *IEEE Trans. Ind. Informat.*, vol. 9, no. 3, pp. 1486–1496, Aug. 2013.

[5] V. Güngör *et al.*, "Smart grid technologies: Communication technologies and standards," *IEEE Trans. Ind. Informat.*, vol. 7, no. 4, pp. 529–539, Nov. 2011.

[6] H. Zhang, F. L. Lewis, and Z. Qu, "Lyapunov, adaptive, and optimal design techniques for cooperative systems on directed communication graphs," *IEEE Trans. Ind. Electron.*, vol. 59, no. 7, pp. 3026–3041, Jul. 2012.

[7] U. Munz, A. Papachristodoulou, and F. Allgower, "Consensus in multi-agent systems with coupling delays and switching topology," *IEEE Trans. Autom. Control*, vol. 56, no. 12, pp. 2976–2982, Dec. 2011.

[8] G. Wen, Z. Duan, W. Ren, and G. Chen, "Distributed Consensus of multi-agent systems with general linear node dynamics and intermittent communications," *Int. J. Robust Nonlinear Control*, vol. 24, no. 16, pp. 2438–2457, 2014.

[9] R. Olfati-Saber, J. A. Fax, and R. M. Murray, "Consensus and cooperation in networked multi-agent systems," *Proc. IEEE*, vol. 95, no. 1, pp. 215–233, Jan. 2007.

[10] R. Olfati-Saber and R. M. Murray, "Consensus problems in networks of agents with switching topology and time-delays," *IEEE Trans. Autom. Control*, vol. 49, no. 9, pp. 1520–1533, Sep. 2004.

[11] B. Wittenmark, J. Nilsson, and M. Törngren, "Timing problems in real-time control systems," in *Proc. Am. Control Conf.*, Jun. 1995, vol. 3, pp. 2000–2004.

[12] J. Nilsson, B. Bernhardsson, and B. Wittenmark, "Stochastic analysis and control of real-time systems with random time delays," *Automatica*, vol. 34, no. 1, pp. 57–64, Jan. 1998.

[13] A. Farraj, E. Hammad, and D. Kundur, "A systematic approach to delay-adaptive control design for smart grids," in *Proc. IEEE Int. Conf. Smart Grid Commun.*, Nov. 2015, pp. 768–773.

[14] K.-D. Kim and P. R. Kumar, "Cyber–physical systems: A perspective at the centennial," *Proc. IEEE*, vol. 100, no. Special Centennial Issue, pp. 1287–1308, May 2012.

[15] J. Song, E. Cotilla-Sanchez, G. Ghanavati, and P. D. Hines, "Dynamic modeling of cascading failure in power systems," *IEEE Trans. Power Syst.*, vol. 31, no. 3, pp. 2085–2095, May 2016.

[16] P. Derler, E. A. Lee, and A. S. Vincentelli, "Modeling cyber–physical systems," *Proc. IEEE*, vol. 100, no. 1, pp. 13–28, Jan. 2012.

[17] F. Cremona, M. Lohstroh, D. Broman, E. A. Lee, M. Masin, and S. Tripakis, "Hybrid co-simulation: It's about time," *Softw. Syst. Model.*, vol. 17, pp. 1–25, 2017.

[18] I. Akkaya, Y. Liu, and E. A. Lee, "Modeling and simulation of network aspects for distributed cyber-physical energy systems," in *Cyber Physical Systems Approach to Smart Electric Power Grid*. New York, NY, USA: Springer, 2015, pp. 1–23.

[19] A. Farraj, E. Hammad, and D. Kundur, "A systematic approach to delay-adaptive control design for smart grids," in *Proc. IEEE Int. Conf. Smart Grid Commun.*, 2015, pp. 768–773.

[20] J. S. Thorp, C. E. Seyler, and A. G. Phadke, "Electromechanical wave propagation in large electric power systems," *IEEE Trans. Circuits Syst. I, Fundam. Theory Appl.*, vol. 45, no. 6, pp. 614–622, Jun. 1998.

[21] L. Huang, M. Parashar, A. Phadke, and J. Thorp, "Impact of electromechanical wave propagation on power system protection and control," in *Proc. CIGRE Conf.*, 2002, pp. 201–206.

[22] S. Backhaus and Y. Liu, "Electromechanical wave green's function estimation from ambient electrical grid frequency noise," in *Proc. Hawaii Int. Conf. Syst. Sci.*, 2012, pp. 2054–2061.

[23] T. Li, G. Ledwich, and Y. Mishra, "Role of electromechanical wave propagation in power systems," in *Proc. Power Energy Soc. General Meeting*, 2013, pp. 1–5.

[24] S.-J. Tsai *et al.*, "Frequency sensitivity and electromechanical propagation simulation study in large power systems," *IEEE Trans. Circuits Syst. I, Reg. Papers*, vol. 54, no. 8, pp. 1819–1828, Aug. 2007.

[25] A. Semlyen, "Analysis of disturbance propagation in power systems based on a homogeneoue dynamic model," *IEEE Trans. Power App. Syst.*, vol. PAS-93, no. 2, pp. 676–684, Mar. 1974.

[26] E. Shehab-Eldin and P. McLaren, "Travelling wave distance protection-problem areas and solutions," *IEEE Trans. Power Del.*, vol. 3, no. 3, pp. 894–902, Jul. 1988.

[27] E. O. Schweitzer, A. Guzmán, M. V. Mynam, V. Skendzic, B. Kasztenny, and S. Marx, "Locating faults by the traveling waves they launch," in *Proc. Annu. Conf. Protective Relay Eng.*, 2014, pp. 95–110.

[28] F. Hohlbaum, M. Braendle, and F. Alvarez, "Practical considerations for implementing iec 62351," PAC World Conference, 2010.
[29] J. Nutaro and V. Protopopescu, "A new model of frequency delay in power systems," *IEEE Trans. Circuits Syst. II, Exp. Briefs*, vol. 59, no. 11, pp. 840–844, Nov. 2012.
[30] P. Pattabi, E. Hammad, A. Farraj, and D. Kundur, "Simplified implementation and control of a flywheel energy system for microgrid applications," in *Proc. IEEE Global Conf. Signal Inf. Process.*, 2017, pp. 1–5.
[31] P. Kundur *et al.*, "Definition and classification of power system stability IEEE/CIGRE joint task force on stability terms and definitions," *IEEE Trans. Power Syst.*, vol. 19, no. 3, pp. 1387–1401, Aug. 2004.
[32] P. Kundur, *Power System Stability and Control* EPRI Power System Engineering Series. New York, NY, USA: McGraw-Hill, 1994.
[33] P. W. Sauer and M. A. Pai, *Power System Dynamics and Stability*. Englewood Cliffs, NJ, USA: Prentice-Hall, 1998.
[34] J. Glover, M. Sarma, and T. Overbye, *Power System Analysis & Design*, 5th ed. Boston, MA, USA: Cengage Learning, 2011.
[35] E. Hammad, A. Farraj, and D. Kundur, "On effective virtual inertia of storage-based distributed control for transient stability," *IEEE Trans. Smart Grid*, vol. 10, no. 1, pp. 327–336, Jan. 2019.
[36] A. Farraj, E. Hammad, and D. Kundur, "A cyber-enabled stabilizing controller for resilient smart grid systems," in *Proc. IEEE PES Conf. Innovative Smart Grid Technol.*, Feb. 2015, pp. 1–5.
[37] E. Hammad, A. Farraj, and D. Kundur, "Paradigms and performance of distributed cyber-enabled control schemes for the smart grid," in *Proc. IEEE Power Energy Soc. General Meeting*, 2015, pp. 1–5.
[38] E. Hammad, A. Farraj, and D. Kundur, "A resilient feedback linearization control scheme for smart grids under cyber-physical disturbances," in *Proc. IEEE PES Conf. Innovative Smart Grid Technol.*, Feb. 2015, pp. 1–5.
[39] E. Hammad, J. Zhao, A. Farraj, and D. Kundur, "Mitigating link insecurities in smart grids via qos multi-constraint routing," in *Proc. IEEE Int. Conf. Commun. Workshops*, 2016, pp. 380–386.
[40] E. Hammad, A. Farraj, and D. Kundur, "On the effects of distributed control area design for the stabilization of cyber-enabled smart grids," in *Proc. Workshop Model. Simul. Cyber-Physical Energy Syst.*, 2015, pp. 1–6.
[41] E. Hammad, A. Farraj, and D. Kundur, "Paradigms and performance of distributed cyber-enabled control schemes for the smart grid," in *Proc. IEEE Power Energy Soc. General Meeting*, 2015, pp. 1–5.
[42] L. Ding, F. M. Gonzalez-Longatt, P. Wall, and V. Terzija, "Two-step spectral clustering controlled islanding algorithm," *IEEE Trans. Power Syst.*, vol. 28, no. 1, pp. 75–84, Feb. 2013.
[43] R. J. Sánchez-García *et al.*, "Hierarchical spectral clustering of power grids," *IEEE Trans. Circuits Syst. I, Reg. Papers*, vol. 29, no. 5, pp. 2229–2237, Sep. 2014.

Eman Hammad received the Ph.D. degree in electrical engineering from the University of Toronto, Toronto, ON, Canada, in 2018.

Her research focuses on the cyber-physical security and resilience of smart power systems. Her work investigates how a deeper understanding of interactions between critical infrastructure systems and enabling technologies can help design new classes of operational solutions that are more resilient to cyber-physical disruptions. Her research interests include cyber-physical security, resilient autonomous systems, operational trust, and cooperative game theory in the context of smart grids. He has published 47 peer-reviewed articles in highly ranked journals and conferences.

Dr. Hammad's research has been recognized by IEEE SmartGridComm '15 Best Paper Award, and the Institute of Sustainable Energy '14 Best Poster Award. She has been an active volunteer with IEEE and is currently serving as the Chair for IEEE Toronto Communication Society Chapter for which she has been awarded the IEEE ComSoc Chapter Achievement Award '18.

Abdallah Farraj received the B.Sc. and M.Sc. degrees in electrical engineering from the University of Jordan, Amman, Jordan, and the Ph.D. degree in electrical engineering from Texas A&M University, Uvalde, TX, USA.

He is a Senior Advisor with PricewaterhouseCoopers. His research interests include security and resilience of critical infrastructure and industrial control systems, modeling and analysis of cyber-physical systems, and cyber security of IT/OT systems.

Deepa Kundur was born in Toronto, Canada. She received the B.A.Sc., M.A.Sc., and Ph.D. degrees all in electrical and computer engineering in 1993, 1995, and 1999, respectively, from the University of Toronto, Toronto, ON, Canada.

She currently serves as a Professor and Director of the Centre for Power & Information, The Edward S. Rogers Sr. Department of Electrical & Computer Engineering, University of Toronto. Her research interests include the interface of cyber security, signal processing, and complex dynamical networks. She is an author of more than 200 journal and conference papers. She is also a recognized authority on cyber security issues and has appeared as an expert in popular television, radio, and print media.

She has participated on several editorial boards and currently serves on the Advisory Board of IEEE Spectrum. She currently serves as the Chair of the Division of Engineering Science as well as the General Chair for the 2018 GlobalSIP Symposium on Information Processing, Learning and Optimization for Smart Energy Infrastructures, and TPC Co-Chair for IEEE SmartGridComm 2018. Recently, she also served as the Symposium Co-Chair for the Communications for the Smart Grid Track of ICC 2017, the General Chair for the Workshop on Communications, Computation and Control for Resilient Smart Energy Systems at ACM e-Energy 2016, the General Chair for the Workshop on Cyber-Physical Smart Grid Security and Resilience at Globecom 2016, the General Chair for the Symposium on Signal and Information Processing for Smart Grid Infrastructures at GlobalSIP 2016, the General Chair for the 2015 International Conference on Smart Grids for Smart Cities, the General Chair for the 2015 Smart Grid Resilience Workshop at IEEE GLOBECOM 2015, and the General Chair for the IEEE GlobalSIP'15 Symposium on Signal and Information Processing for Optimizing Future Energy Systems. She has received best paper recognitions at numerous venues including the 2015 IEEE Smart Grid Communications Conference, the 2015 IEEE Electrical Power and Energy Conference, the 2012 IEEE Canadian Conference on Electrical & Computer Engineering, the 2011 Cyber Security and Information Intelligence Research Workshop, and the 2008 IEEE INFOCOM Workshop on Mission Critical Networks. She has also been the recipient of teaching awards at both the University of Toronto and Texas A&M University. She is a Fellow of the Canadian Academy of Engineering.